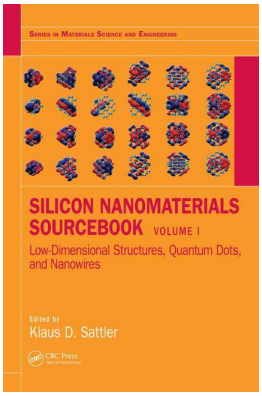

Silicon Nanomaterials Sourcebook
Low-Dimensional Structures Nanopowders, Nanowires

Klaus D. Sattler

Surface-engineered silicon nanocrystals

Publication details
https://test.routledgehandbooks.com/doi/10.4324/9781315153544-16
Calum McDonald, Tamilselvan Velusamy, Davide Mariotti, Vladimir Svrcek
Published online on: 09 Aug 2017

14 Surface-engineered silicon nanocrystals

Calum McDonald, Tamilselvan Velusamy, Davide Mariotti, and Vladimir Svrcek

Contents

14.1 Introduction 323
14.1.1 The Importance of Silicon with Quantum Confinement 323
14.1.2 Compatibility within Photovoltaics 325
14.1.3 On the Origin of PL in SiNCs 325
14.1.4 Quantum-Confined Silicon 326
14.1.5 Surface Properties 326
14.2 SiNC Surface Engineering Techniques 328
14.2.1 Ligand Surface Attachment 328
14.2.1.1 Hydrosilylation 329
14.2.1.2 Advantages and Disadvantages 329
14.2.2 Inorganic Shells 329
14.2.2.1 Advantages and Disadvantages 330
14.2.3 Surface Engineering by Plasma–Liquid Chemistry 330
14.2.3.1 Plasma Generated by Laser 330
14.2.3.2 Plasmas Generated in Gas 331
14.2.3.3 Advantages and Disadvantages 331
14.3 Surface Engineering of Doped SiNCs in Liquid Plasma 331
14.3.1 p-Type SiNCs 331
14.3.2 n-Type SiNCs 332
14.4 Surface-Engineered SiNC in Photovoltaic Devices 335
14.5 Conclusion 337
Acknowledgment 337
References 337

14.1 INTRODUCTION

14.1.1 THE IMPORTANCE OF SILICON WITH QUANTUM CONFINEMENT

When the radius of a nanoparticle is reduced below its Bohr exciton radius, the nanoparticle electronic energy structure becomes confined, leading to a set of unique properties which enable a range of new applications. Quantum confinement is generally observed in the widening of the band gap, where the band gap energy becomes inversely proportional to particle size. The possibility to tune the energy gap by controlling particle size is an intriguing and exciting aspect of quantum-confined materials, which allows us to fine-tune material properties as per application requirements. In addition to an increase in the band gap energy, other changes following quantum confinement of the energy structure are as follows: a change in the oscillator strength; an enhancement of carrier life times, necessary for carrier

multiplication or hot-carrier extraction; and a change in transition dynamics, for example, a shift toward direct band gap behavior for silicon.

As well as the particle size, the surface properties require important considerations for quantum-confined nanocrystals. Due to the high surface-to-volume ratio, which exists in zero-dimensional nanostructures, the influence of surface states on the overall properties becomes significant. At the surface of a nanocrystal, atoms experience vastly different conditions than at the core, such as increased strain, changes to crystal structure, and variations in surface terminations. Surface terminations play a vital role in nanocrystal properties, and therefore surface termination of an SiNC must be considered. SiNCs exhibit a wavefunction which overlaps with the surface states and thus the surface terminations influence the wavefunction of the core and therefore the energy structure. The surface termination of SiNCs has also been well demonstrated to affect both the photoluminescence (PL) intensity and energy, and the absorption properties of the nanocrystal. The PL and absorption properties of a nanocrystal are usually a good indicator of the surface properties; however, it is important to note that in the case of SiNCs it is sometimes insufficient to distinguish between Si–C and Si–H terminations. PL emission from an indirect gap semiconductor such as Si is an interesting property in itself, given that a radiative recombination via an indirect transition requires the absorption or emission of a phonon in order to conserve crystal momentum. Certainly, different surface terminations are well observed to vary PL energy, while reducing particle size is also observed to strongly influence PL emission.

Following most synthesis techniques, SiNCs typically exhibit a hydride, halogen, or oxide surface, depending on the synthesis route. H-terminated SiNCs have large spectral tunability and are well-studied, but are chemically unstable and readily oxidize. In general, H terminations on SiNCs will be replaced by a hydroxyl/oxide termination in the presence of water. OH terminations provide a higher degree of passivation than H-terminated surfaces, are more stable than H terminated SiNCs, and display an enhanced PL intensity. However, over time, OH-terminated SiNCs will oxidize.

Oxidized SiNCs, while optically and chemically stable, have a red-shifted PL, a low PL quantum yield, low radiative rates, are difficult to surface engineer, and completely oxidized SiNCs have been shown to possess delocalized electronic states.[1] However, surface oxidation of SiNCs has been shown to improve the performance of SiNCs in solar cells.[2] As-prepared SiNCs often contain dangling bonds which act as carrier traps, while an oxidized surface favorably replaces dangling bonds with Si–O–Si bridge bonds and reduces carrier traps. It was well-noted by Ding et al.[2] that the amount of oxidation played a vital role in determining the effectiveness of the SiNCs in a hybrid solar cell; an oxidized SiNC surface was shown to improve solar cell device performance, while an excessively oxidized surface deteriorated the electrical properties and hampered device performance. Therefore, techniques for inducing oxide layer growth in a controlled manner are desirable.

In this chapter, we will see that SiNC properties are strongly dependent on the surface, and methods to modify surface terminations will be outlined. In particular, freestanding SiNCs will be discussed, where "freestanding" refers to unsupported SiNCs which are neither grown within a solid matrix nor on a solid substrate. While both freestanding nanocrystals and those supported by a matrix or on a substrate have individual merits, the latter two types do not have their surfaces exposed, and therefore access to the surface is not convenient which makes it difficult to tune their properties by surface engineering. Freestanding SiNCs refer to nanocrystals which are produced in liquid/gas phases or have been released from solid matrices, and are preferential for studies regarding surface engineering due to the ease of access to their surfaces. Therefore, since this chapter is concerned with the surface engineering of SiNCs, we will focus on freestanding nanocrystals.

Different types of surface terminations for SiNCs include short-chain terminations, ligands, and inorganic semiconductor coatings. Various wet-chemical methods exist, particularly for ligand attachment and termination with halides, however, these types of terminations are either unsuitable for electronic devices or highly unstable. The story emerging is that a controlled oxide layer on an SiNC is desirable for both passivating SiNCs while also maintaining the excellent optoelectronic properties of SiNCs. Probably the most effective and simple method to achieve surface passivation without long-chain ligands is the liquid–plasma

chemistry method. This method can be used to produce conductive and stable SiNCs, modify the Fermi level, and enhance PL intensity.

14.1.2 COMPATIBILITY WITHIN PHOTOVOLTAICS

SiNCs are of particular interest due to the nature of the preexisting electronics industry, which is largely based on silicon wafer technology. The ability to combine SiNCs with Si-wafer technology is of paramount interest and poses the most significant application opportunity and development route for SiNCs in the near future. Since a well-established infrastructure for Si-based technologies already exists, it is unlikely that manufacturers will be persuaded to move away from this industry given their commitment and investment. Therefore, while silicon wafer technology still dominates, industrial investment is more likely to be available for technologies which expand on what is already available, without requiring any significant change. In addition, there is already a plethora of knowledge regarding the industrial production of high-quality crystalline silicon and the processing of raw materials, precursors, storage, and waste; to change to a new material would be a substantial move and require huge commitment across all steps of production. Currently, while silicon is so dominant and well established, integration of SiNCs in existing silicon wafer-based devices is most practical.

Examples of possible applications of SiNCs on Si-wafer technology are light-emitting devices,[3] flash memory,[4] solar cells,[5,6] single-electron devices,[7,8] and spintronics.[9] Many of these examples regard SiNCs grown in a solid matrix and therefore cannot be surface engineered, therefore the properties of the SiNCs cannot be optimized. One of the benefits of using SiNCs with bulk silicon photovoltaics (PV) is entailed in the larger band gap of SiNCs. Bulk silicon PV has a band gap of 1.1 eV and a wide absorption spectrum across the visible range of the solar spectrum. Photons absorbed with energy in excess of 1.1 eV generate hot carriers, and excess energy is lost through thermalization (i.e., phonon scattering) as carriers relax to the conduction band edge. Because of this, the optimum band gap energy for a single gap solar cell is roughly 1.5 eV. By employing a wider band gap material such as SiNCs on top of the Si wafer, it is possible to capture and make use of the high-energy light which is not used efficiently by bulk Si solar cells.

Another benefit of quantum-confined SiNCs is carrier multiplication: the process by which photons with energy equal or greater than twice the band gap of the nanocrystal can generate a second carrier via impact ionization. This is an effect observed minutely in all semiconductors under high-intensity illumination of at least twice the band gap energy; however, the process is profoundly inefficient such that there is no noticeable benefit. The effect is far more pronounced in semiconductors with quantum confinement due to the greater separation in the energy of available states, meaning that the relaxation of hot carriers must occur via a multiphonon scattering process, the probability for which is very low. Carrier lifetimes in quantum dots is therefore much higher than in bulk materials, which can theoretically increase the efficiency of solar cells significantly via the process of carrier multiplication.

In the context of photovoltaic applications, one of the drawbacks of SiNCs is the large band gap in the strong quantum confinement regime. Small particle sizes are highly desirable as this increases absorption cross section, carrier lifetimes, and exciton dissociation. However, these small SiNCs with diameters around 2–3 nm have a very large band gap close to or above 3 eV, which is not suitable for third generation photovoltaic concepts.[10] SiNCs with such a large band gap would capture a very small portion of the solar spectrum and carrier multiplication would be irrelevant, as this would require the absorption of photons with energy >6 eV for SiNCs with a band gap of 3 eV. If SiNCs are to be implemented into a photovoltaic device, a smaller band gap is required while maintaining the favorable properties intrinsic to quantum confinement. A smaller band gap is achieved for SiNC with larger diameters, however, this introduces surface defects and dangling bonds which must be well passivated through surface engineering. Therefore, tailoring absorption properties of SiNCs while retaining strong electronic transport and surface passivation is certainly a major challenge for the materials community.

14.1.3 ON THE ORIGIN OF PL IN SiNCs

Interest in SiNCs increased significantly following the report of red PL in electrochemically etched silicon by Canham et al. in 1990.[11] The discovery of bright PL in SiNCs is particularly interesting given that bulk silicon is highly inefficient at emitting light. As silicon is an indirect band gap semiconductor, light

absorption and emission requires the simultaneous absorption or emission of a phonon in order to preserve crystal momentum[12]; therefore recombination in bulk silicon is largely nonradiative.

The exact origin of bright PL in quantum-confined Si has been the subject of discussion for the past two decades,[13–18] and is typically assigned to two models; (1) the quantum confinement model and (2) the surface chemistry model. In the quantum confinement model, the PL is attributed to the quantization of the electronic energy structure within the core of the nanocrystals. Evidence supporting the quantum confinement model has been reported.[16,19–28] In the surface chemistry model, the PL is attributed to highly localized surface defect states; excited carriers in the core states relax into lower lying defect states that slowly radiate. This model is supported experimentally in the literature.[16,24,29–31] Nonetheless, both size and surface termination certainly contribute to the energy and intensity of the PL.

14.1.4 QUANTUM-CONFINED SILICON

The Bohr exciton radius is about 4.2–4.6 nm for Si,[32] and quantum confinement has been shown to increase the indirect band gap from 1.1 eV in bulk silicon up to in excess of 3 eV for particles of ~2 nm diameter.[29,33] Quantum efficiencies approaching that of direct transitions have been observed[33,34]; as the indirect gap is increased, the direct gap is simultaneously decreased (from 3.32 eV) with increasing quantum confinement. In bulk silicon, the direct gap is skipped and electrons relax into the conduction band edge at the indirect gap very quickly. For quantum-confined SiNCs, as the particle size is reduced the indirect gap increases and direct gap decreases, leading to a change in the transition dynamics as direct transitions become more favorable.

Calculated band gap energies for SiNCs embedded in a lattice with varying sizes of the quantum structure are shown in Figure 14.1.[35–38] For structures with diameters <3 nm, there is an exponential increase in the band gap energy as the diameter is reduced further, and SiNCs with diameters of 2 nm are expected to have band gap as large as >3 eV, in agreement with the experimental results discussed above.[29,33] The increase in band gap energy must be accompanied by a shift in the position of valence and conduction band edges; this can be experimentally observed using X-ray and ultraviolet photoelectron spectroscopy techniques, and can be confirmed with effective mass approximation for the band edges.[39]

14.1.5 SURFACE PROPERTIES

While particle size has been demonstrated to determine the energy structure of a nanocrystal, the optical properties, particularly the PL, are also strongly influenced by the surface functionalization process. The optical properties of quantum-confined SiNCs are highly influenced by atoms/molecules/radicals, or

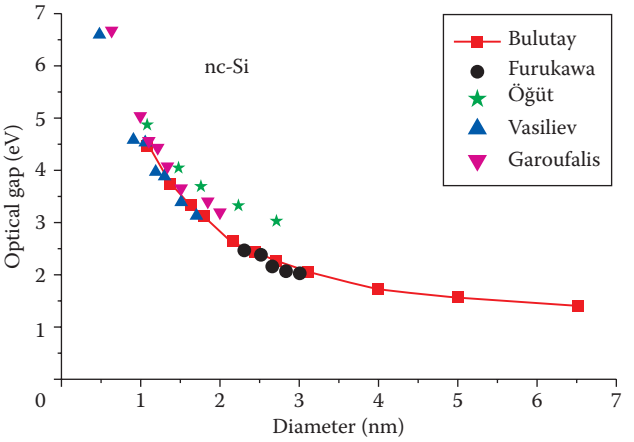

Figure 14.1 Theoretical and experimental band gap trend of quantum-confined SiNCs with H terminations in a matrix reported. (Reproduced from Bulutay, C., *Phys. Rev. B*, 76, 205321, 2007; initial data are reported elsewhere Öğüt, S., et al., *Phys. Rev. Lett.*, 79, 1770–1773, 1997; Vasiliev, I., et al., *Phys. Rev. Lett.*, 86, 1813–1816, 2001; Furukawa, S., and Miyasato, T., *Phys. Rev. B*, 38, 5726–5729, 1988.)

defects at or close to the surface. It is also worth noting that certain surface terminations play an important role in the stability, dispersity, and biocompatibility of the SiNCs in various media. Hydride-terminated SiNCs are not soluble in water; for water-soluble SiNCs, the nanocrystals must be functionalized with polar molecules. Hydride-terminated SiNCs are typically difficult to disperse in common solvents such as water. Toxicity and biocompatibility are also largely determined by the surface terminations; since certain ligand terminations are cytotoxic, they are not compatible in biological applications. Hence, the importance of surface functionalization goes well beyond electronic and optical properties. Surface engineering becomes highly important for integration in devices as it allows: (1) the passivation of the nanocrystal, (2) the tailoring of the optical and electronic properties, and (3) control of mixing/integration/compatibility. However, for the most part, the stability and the electrical and optical properties of the nanocrystal are considered first, while the challenges of integration and compatibility are addressed later. Therefore, this chapter will focus on (1) and (2).

Surface effects in nanocrystals concerning optical properties arise from two fundamental mechanisms:

1. The wavefunctions of carriers in the nanocrystals are delocalized over the whole nanocrystal to include its surface, and therefore the surface wavefunctions interact with the core nanocrystal wavefunction.
2. Due to the small volume of the SiNCs, carriers can easily diffuse to/from the core/surface of the nanocrystal.

The change in PL can arise from changes to surface chemistry, allowing for the tuning of particle properties not only through SiNC size. For example, PL tuning of SiNCs has been demonstrated by the attachment of surface ligands.[29,31,40,41] Differences in surface passivation have been reported to shift the PL emission of similar-sized SiNCs by up to 400 nm in wavelength.[29,31,41] Figure 14.2 shows the change in PL position for SiNCs terminated with different halides. Despite the large spectral tunability available with halides, this type of functionalization is highly unstable due to the reactivity of halides.

While varying surface terminations have been demonstrated to control the PL energy for SiNCs, PL tuning via particle size is still possible even for surfaces functionalized with long organic chains. K. Cheng et al. demonstrated that, for SiNCs synthesized via nonthermal plasma and with 1-dodecene surface terminations, the typical blue shift in PL is still observed as particle size is reduced.[42] The peak PL emission wavelengths were reported as 853 nm and 777 nm for SiNCs with diameters of 5 nm and 3 nm, respectively. The observed PL energy is far smaller than what is expected for H-terminated SiNCs, and the lower PL energy is attributed to recombination via surface ligands. This demonstrates that it is still possible to tune the band gap via particle size even when the surface is highly functionalized. Comparatively, for

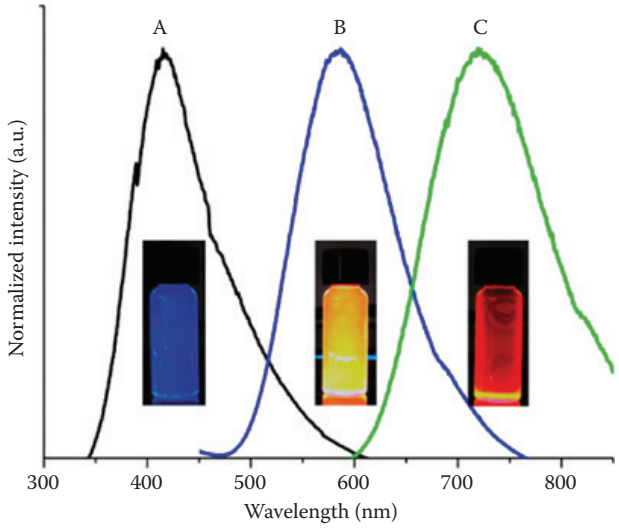

Figure 14.2 The photoluminescence spectra of hexyl-functionalized SiNCs in toluene with (A) chloride, (B) iodide, and (C) bromide surface terminations with particle diameters of approximately 3 nm. (From Dasog, M., et al., *Chem. Mater.*, 27, 1153–1156, 2015.)

H-terminated SiNCs, a reduction in particle size also leads to an increase and blue shift of the excitonic emission intensity.

14.2 SiNC SURFACE ENGINEERING TECHNIQUES

The initial surface termination plays an important role in the surface engineering process. The surface termination present on an SiNC is determined both by the synthesis route and the precursors used. Various methods exist for the synthesis of SiNCs; reduction of silicon halides,[43] steric stabilization,[33] oxidation of Zintl phases,[44] plasma-assisted magnetron sputtering,[45] atmospheric pressure plasma,[46–49] hydrosilylation,[50] and electrochemical etching.[51] Of the widely employed synthesis methods for SiNCs, the majority yield particles with a surface terminated by a hydride, halogen, or oxide. Therefore, the surface engineering technique should be compatible with these surfaces. In this section, several prominent methods for surface engineering will be discussed.

14.2.1 LIGAND SURFACE ATTACHMENT

The functionalization of SiNCs with ligands is a popular method for surface engineering as there is a vast array of possible ligand attachments, which allows for a significant amount of control over surface properties. Ligand attachment can stabilize the surface of the nanocrystals and provide steric hindrance. Alkanes, which are the simplest organic ligands consisting of only carbon and hydrogen, are the most commonly investigated ligand for surface functionalization, and can be easily attached to the surface of SiNCs via the hydrosilylation of an alkyl radical. Alkyl-terminated SiNCs are stable due to strong Si–C bonds which prevent photooxidation, provide steric protection, and also avert aggregation when in solution.

Alkyl chains tend to have a minimum effect on the optical gap of SiNCs because of the often type-I alignment of the energy levels. In type-I alignment, both the electron and hole are confined in the core, while in type-II alignment, one carrier is mostly confined to the shell and the other mostly confined to the core. Type-I alignment occurs when the highest occupied molecular orbital (HOMO) and lowest unoccupied molecular orbital (LUMO) of the core exist within the band gap of the shell energy levels, and have a minimal effect on the optical gap of the SiNCs.[40] Type-II band alignment is achieved, for example, through an energy band alignment in which both the HOMO and LUMO of the core are lower than their respective shell energy levels. This is shown schematically in Figure 14.3. Both type-I and type-II

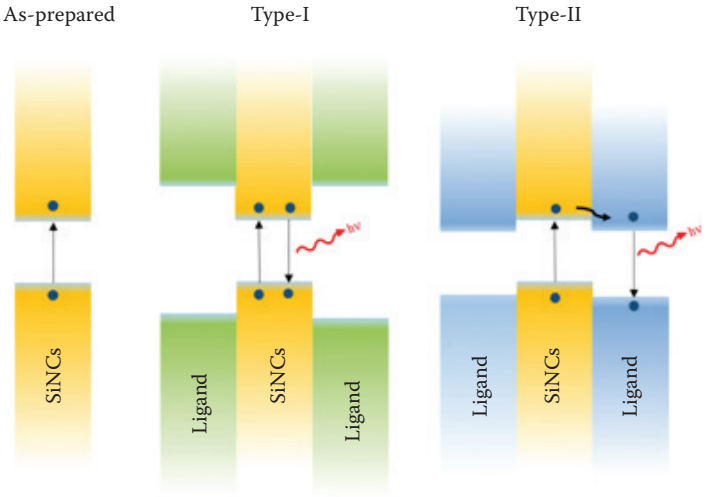

Figure 14.3 Band alignment for as-prepared silicon nanocrystals (SiNCs) and SiNCs with type-I alignment and type-II alignment via surface ligand functionalization. In a type-I alignment, the carriers are confined to the SiNCs and recombination occurs within the core, while in a type-II alignment the carriers can relax into the LUMO of the ligand and recombine.

alignments are possible with SiNCs, and type-II alignment can be used to modify the optical properties of the SiNC, which has been previously demonstrated.[52] In this manner, it is possible to control the optical properties without changing particle size and by only changing the ligand.

14.2.1.1 Hydrosilylation

Hydrosilylation is one of the most widely used methods for the attachment of alkyls to SiNC surfaces due to its simplicity, and involves the replacement of a typically H-terminated SiNC surface with Si–C, Si–O, Si–N, or Si–S bonds. Si–C bonds are predominantly favorable due to strong resistance to oxidation and compatibility with organic compounds, allowing the formation of surface-functionalized SiNCs with ligands.

The two most common types of hydrosilylation employed are thermal and photochemical hydrosilylation. Thermally induced hydrosilylation occurs via the thermally initiated cleavage of Si–H bonds followed by the formation of an Si–C bond. Thermal hydrosilylation is independent of particle size and does not require a catalyst, however, high reaction temperatures are necessary which limits the selection of alkenes and alkynes to those which can withstand such temperatures. Photochemical hydrosilylation occurs via UV-light-induced cleavage of Si–H bonds. Photochemical hydrosilylation can be performed at room temperature and in various solvents, which determines the type of surface functionalization obtained.

14.2.1.2 Advantages and disadvantages

The main advantage of both thermally and photochemically induced hydrosilylation is the ease and simplicity of the procedure. These techniques do not require much equipment and are therefore inexpensive and simple to set up. There is also a wide array of possible surface functionalization available owing to a high degree of tunability in terms of optical properties, solubility, and biocompatibility. This presents many opportunities for applications in biolabeling, for example, and thus a large amount of research interest exists in the hydrosilylation of SiNCs.

One of the major issues with hydrosilylation is that the attachment of long-chain alkyls inhibits the performance of SiNCs in electronic devices. Long-chain organic terminations are a hindrance particularly for electronic devices which require good transport properties. Ligands are not suitable for electronic devices as they inhibit certain electronic processes, such as carrier transport properties and exciton dissociation in photovoltaic devices. In order to produce useful electronic devices from ligand-terminated SiNCs, the electrically insulating native ligands must be exchanged in order to produce conductive SiNC arrays, introducing significant complexity into the fabrication process.

In addition to this, it is difficult to cover the entire surface of the particle uniformly with ligands, leading to irregularities in properties and stability; any untreated surfaces offer opportunities for inward oxidation. Thermal hydrosilylation is not effective for short-chain alkyls and is limited to alkyls which can withstand the high reaction temperatures necessary for thermal hydrosilylation, while the reaction dynamics and outcome of photochemical hydrosilylation is dependent on the initial particle size, and is not effective for particles with diameters >5 nm. Photochemical hydrosilylation reaction times are long, typically around a few days, and result in a decrease in initial particle size which must be factored in when designing surface engineering experiments.

14.2.2 INORGANIC SHELLS

The coating of SiNCs with inorganic shells is a remarkable yet highly challenging method for the control of SiNC surface properties. In this method, semiconductor quantum dots are typically contained within the shell of a semiconductor material. Like ligand attachment, this can be achieved in a type-I or type-II alignment, determined by the energy structure of the shell material relative to the SiNC. The type of alignment selected will depend on the properties of the SiNC that are desired.

SiNCs coated with CdS have been reported,[53] forming a type-II nanocrystal; absorption occurs via a transition within the core SiNC and recombination occurs via a transition in the CdS shell. In this work, SiNCs were synthesized initially by hydrogen reduction of $HSiO_{1.5}$ forming an Si–SiO_2 composite. The SiNCs were then removed by HF etching to yield H- and F-terminated SiNCs. Following extraction reflux, the SiNCs were capped with 1-decene to improve dispersion. The CdS shell was then grown by a successive ion layer adhesion and reaction (SILAR) technique. This work showed that the spectroscopic properties and

the electrical conductivity of the Si–CdS nanocrystals can be controlled by varying the thickness of the CdS shell. Specifically, the absorption onset for Si–CdS NCs was reduced to a lower energy for a thicker CdS shell, though this is highly likely due to increased CdS absorption. PL decay times still indicated that the transition for thicker CdS shells remained within the shell.

14.2.2.1 Advantages and disadvantages

Inorganic shell coatings present an excellent method to passivate the SiNC surface. Since SiNCs easily oxidize, it is possible to select shell materials which are less prone to oxidation than Si. However, while the SILAR technique is quite simplistic in itself, it is rather limited with regard to which shell materials can be grown; typically, binary II–VI compounds such as CdS and ZnS. Currently, only type-II core-shell SiNCs have been reported using CdS, likely due to the limited compatibility of the SILAR method. In addition, the use of the toxic element cadmium defeats the ecological benefits of using silicon. The growth of other types of semiconductor shells is challenging and requires the development of many new techniques and understanding for growing uniform shells on nanocrystal surfaces with complete coverage.

For solar energy applications, the large band gap of SiNCs is unattractive as it does not match well with the solar spectrum. Since in type-II alignment the absorption occurs in the SiNC, the amount of energy harvestable will be very low, greatly reducing the efficiency of the device. As stated earlier, small SiNCs (1–3 nm) are desirable due to high-absorption cross sections, enhanced exciton transport, and higher carrier lifetimes. However, we have also seen that such small SiNCs have very large band gaps, unsuitable for solar energy applications. To address this, a transition from the HOMO of a surface state to the LUMO of the SiNC can generate an absorption edge lower than the band gap of SiNCs. This can be achieved via type-II alignment, and would require careful materials selection in order to correctly align the band energies of the materials; however, these materials may not necessarily be compatible with the SILAR method.

14.2.3 SURFACE ENGINEERING BY PLASMA–LIQUID CHEMISTRY

In this section, the surface functionalization of freestanding SiNCs in liquid media by atmospheric pressure microplasma will be presented. This type of surface engineering can be carried out during or post synthesis, while wet-chemical methods like hydrosilylation are mostly performed post synthesis. In this technique, the surface engineering of nanocrystals is carried out directly in a colloid, where the liquid media can be a wide range of solvents yielding different surface chemistries; however, this chapter will focus on the surface engineering in ethanol and water. A chemically active surface is required for plasma–liquid surface engineering, for example, Si–H, Si–OH, Si–Cl terminations, and the starting surface termination can determine the type of engineering achieved. Si–H terminations can be readily achieved following synthesis via electrochemical etching in hydrofluoric acid. Three main methods have been developed for surface engineering by atmospheric pressure plasma in liquid media; pulsed laser processes, direct-current (DC) plasma, and ultrahigh frequency (UHF) plasma.[54]

14.2.3.1 Plasma generated by laser

The laser-based surface engineering method uses a pulsed laser to generate a plasma plume in the colloidal solution. This technique is a combined fragmentation and surface engineering process which can be achieved with many types of lasers and is compatible with a wide range of solvents. This process is performed at room temperature for different time scales (from a few minutes to a few hours). The focal spot size of the laser used is typically 3 mm in diameter, with a focal length of 250 mm. Photothermal heating and Coulomb explosion processes occur in the colloidal solution which fragment the SiNCs and generate the plasma. The resulting surface chemistry obtained depends highly on the solvent used and is sensitive to the processing time. For water, this process transforms Si–H bonds to Si–OH after 15 min processing, and following 45 min processing, inward oxide growth commences at Si–Si back bonds and Si dimers observed by a decrease in PL intensity. Due to the stable oxygen-based terminations on the SiNCs after 15 min processing, oxide growth must be facilitated by strained bonds due to Si-dimers present on the SiNC surface. This undesirable slow oxide growth introduces further defects into the SiNC surface which reduces the SiNC core size and deteriorates PL properties. For surface engineering in ethanol, the process favors

Si–OH formation and yields a higher PL intensity and red shift. The growth of an oxide layer is restricted for surface engineering in ethanol and thus the PL properties are more stable.[47]

14.2.3.2 Plasmas generated in gas

This section will discuss both DC and UHF methods of microplasma-induced surface engineering. The resulting chemistries and surface engineering are very similar for both DC and UHF plasma treatment.[55–57] Both plasma processes stabilize the optical properties of the SiNCs and prevent degradation of the PL intensity even for SiNCs processed in water. For surface engineering in water, these methods produce hydrogen peroxide (H_2O_2) which contributes to the removal of surface defects and surface oxidation in combination with other chemical processes. In water, there is no observed shift in PL position for both DC and UHF processes.

In the DC atmospheric pressure plasma method, a plasma is generated between a metal tube and the surface of the colloid. The metal tube is made of either nickel or stainless steel, with an internal diameter of typically either 0.7 mm or 0.25 mm, and the plasma is generated between the metal tube and the surface of the colloid. A counter electrode is also used, which is made of either a carbon rod or metal wire, and is inserted approximately 5 mm in the solution, approximately 2 cm from the metal tube. The plasma is achieved using either pure He or Ar gas at a flow rate of 25–100 sccm with a constant current of 0.5–5 mA applied. The distance from the metal tube to the colloid is 0.5–1 mm, and this distance is adjusted throughout the reaction to account for solvent evaporation. The SiNC concentration in the colloidal solution, the type of solvent used, and the processing current all affect the outcome of the surface engineering process. Since the plasma is created between the metal tubing and the grounded solution, it is necessary for the colloid to be somewhat conductive in order to achieve a plasma. This is a slight disadvantage to this method and limits its applicability and flexibility, and therefore the UHF method was developed in which the plasma is generated within a quartz tube independent of the solution.[55–58]

In the UHF method, also referred to as the radio frequency (RF) method, a plasma is generated within a quartz capillary tube. The plasma can be generated independent of a counter electrode, and the process can be carried out with non-conductive colloids. The distance from the capillary tube to the surface of the colloid is 2 mm initially, which was also adjusted according to solvent evaporation. Although the resultant surface engineering is effectively the same, the physical processes involved in DC and UHF plasma processing are quite different.

14.2.3.3 Advantages and disadvantages

As these methods can be carried out in colloidal solution, they have the benefit of easy storage, and can be deposited at low cost via spin coating, screen printing, and spray coating. However, the experimental setup is more complicated than the wet-chemical methods, and therefore requires expertise in plasma configuration. The DC and UHF methods are not sufficient at fragmenting SiNCs, while the laser method is capable of highly fragmenting the SiNCs into small spherical particles, which is particularly useful for applications in electronic devices. However, the type of surface engineering achieved through the laser method is highly susceptible to reaction times and must be optimized accordingly.

14.3 SURFACE ENGINEERING OF DOPED SiNCs IN LIQUID PLASMA

In this section, we will discuss the surface engineering of p- and n-type SiNCs by atmospheric pressure plasma in liquid.

14.3.1 p-TYPE SiNCs

The surface engineering of p-type SiNCs has been studied in DC and RF plasma, and it is observed that both processes result in the same surface engineering.[55–58] DC and RF plasma processes in water produce mostly OH^- ions and OH radicals, and a small concentration of H_2O_2. SiNCs synthesized via electrochemical etching are H terminated with occasional Si dimers and dangling bonds. The surface engineering of H-terminated p-type SiNCs in water leads to the transformation of H terminations to OH terminations

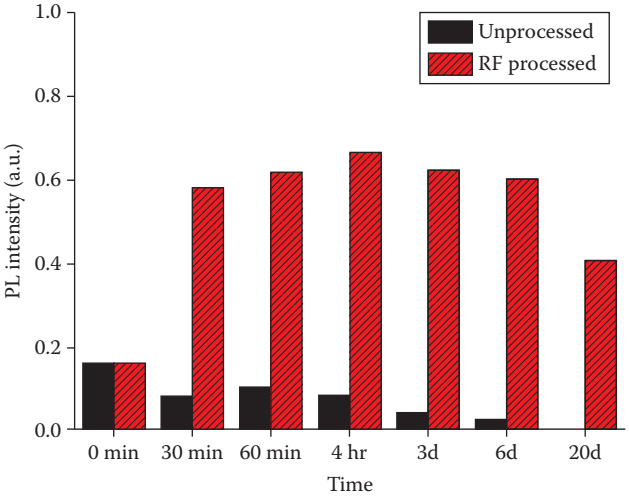

Figure 14.4 Enhanced photoluminescence stability of RF microplasma surface-engineered p-type silicon nanocrystals in water. (From Mitra, S., et al., *Plasma Process. Polym.*, 11, 158–163, 2014.)

via the highly reactive OH^- and OH species. These OH terminations in turn condensate into a thin surface oxide layer, preventing further inward oxidation. It was found that H_2O_2 can cleave Si back bonds of H-terminated SiNCs leading to inward oxidation; however, the rate of H_2O_2 formation is expected to be much lower than the formation of OH^- and OH species. The effect of surface engineering on p-type SiNCs in water is shown in Figure 14.4. The PL intensity is significantly increased owed to the formation of Si–O terminations and is stable over a period of 20 days.

In the case of plasma processing in ethanol, CH_3CH_2OH is dissociated into $CH_3CH_2O^- + H^\bullet$. For p-type SiNCs with H terminations, these $CH_3CH_2O^-$ radicals can replace H terminations on SiNCs with $Si–O–C_2H_5$. Water and ethanol processing both yield SiNCs with similar peak PL, with a higher peak PL intensity observed for surface engineering carried out in water. The higher PL intensity is attributed to the formation of R–O terminations for surface engineering in water which presents a recombination pathway. This oxidation occurs very slowly in ethanol, possibly because of a small presence of water in the ethanol.

14.3.2 n-TYPE SiNCs

While the surface engineering of p-type SiNCs is established, n-type engineering is not well understood. Both p- and n-type SiNCs are required for particular electronic devices, and therefore an understanding of the engineering of both types is necessary. Velusamy et al. reported drastically different properties for the surface engineering of p- and n-type SiNCs under the same conditions.[59]

The differences in n-type and p-type SiNC surface engineering is shown schematically in Figure 14.5. The dissimilarities in surface termination can be attributed to the different types of allowed reactions which can take place at the surface of the SiNC. In short, a p-type surface exhibits surface holes (i.e., positively charged) while an n-type surface is electron rich. Thus, in the case of p-type SiNCs, the positively charged surface can react with negatively charged ions present in the solution (e.g., $CH_3CH_2O^-$ in the case of ethanol) formed due to the plasma. These Si–H terminations are replaced with more stable Si–O–R terminations. For n-type SiNCs, due to the electron-rich surface, the reaction of negatively charged ions is prohibited. Instead, slower reactions with OH, H_2O_2, and H_2O likely lead to the formation of $Si\text{-}H_x$, O_2SiH_2, and a surface oxide network of Si–O–Si bonds.

The effect of surface engineering on the PL spectrum of n- and p-type SiNCs is shown in Figure 14.5. As-prepared n- and p-type SiNCs both exhibit low PL intensity with the PL peak observed at roughly 600 nm and 550 nm, respectively. Following surface engineering in ethanol, the PL intensity of both n- and p-type SiNCs was enhanced dramatically. For surface-engineered n-type SiNCs, the peak PL position was red shifted by approximately 105 nm to 700 nm, while the peak PL of p-type SiNCs was red shifted by

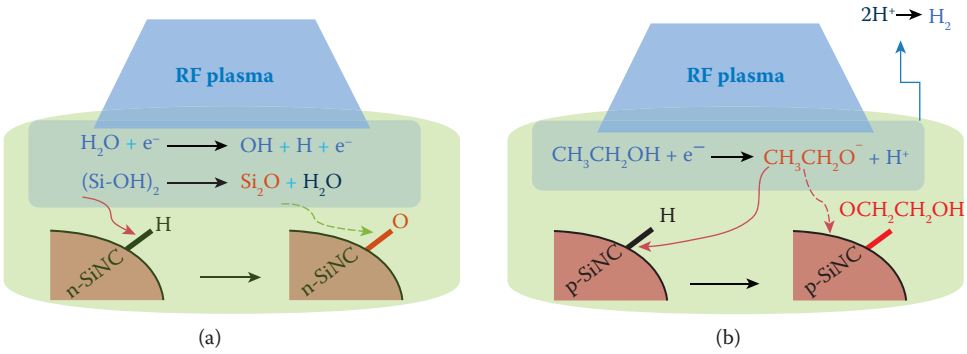

Figure 14.5 Comparison between the surface engineering of (a) n-type and (b) p-type silicon nanocrystals in ethanol. (From Velusamy, T., et al., *ACS Appl. Mater. Interfaces* 7, 28207–28214, 2015.)

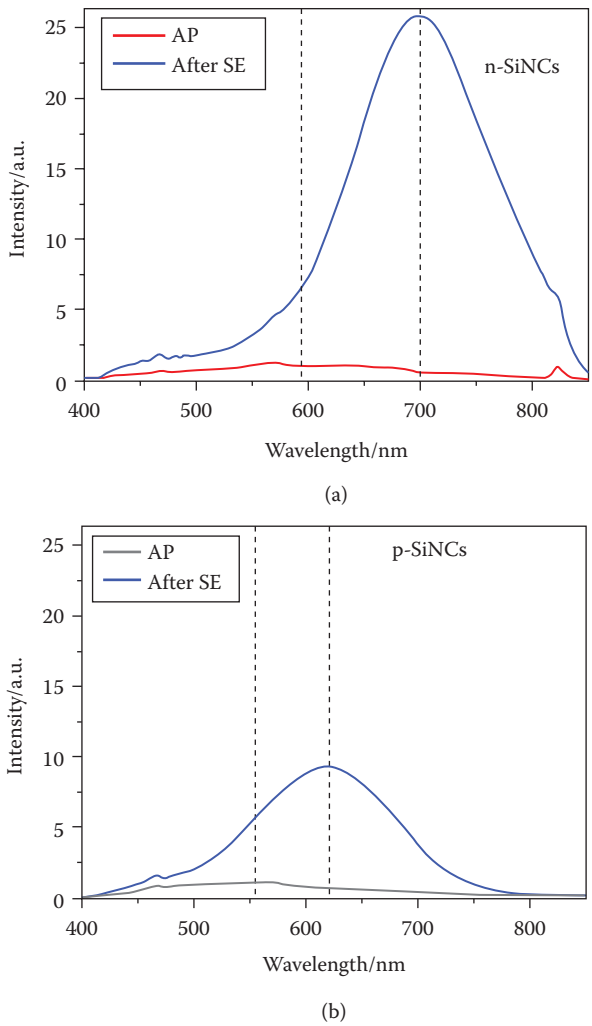

Figure 14.6 Photoluminescene (PL) spectra for as-prepared and for surface-engineered (SE) (a) n-type and (b) p-type silicon nanocrystals (SiNCs) in ethanol. The dotted lines indicate the PL maximum. (From Velusamy, T., et al., *ACS Appl. Mater. Interfaces* 7, 28207–28214, 2015.)

approximately 70 nm to 620 nm. The significant increase in PL intensity is attributed to the formation of a surface oxide layer following surface engineering, presenting a recombination route for carriers via localized oxygen surface states. A red shift in peak PL position is well observed in the literature for oxidized SiNCs, which is in agreement with the results shown in Figure 14.6 for both n- and p-type SiNCs. A higher degree of oxidation is indicated by a greater red shift. The red shift observed for n-type SiNCs is greater than that of p-type SiNCs, indicative of a higher degree of oxidation. Following surface engineering, p-type SiNCs tend to exhibit OH- and R–O-terminations, while n-type SiNCs exhibit Si–O–Si oxide network, which was observed in Fourier transform infrared spectroscopy measurements.

A comparison of the PL stability is shown in Figure 14.7. The PL of surface-engineered n-type SiNCs is far less stable than the PL of p-type SiNCs. After storage for 7 days in ethanol, the peak PL of n-type SiNCs is blue shifted by approximately 70 nm and the PL intensity is significantly lower. For p-type SiNCs, the PL is blue shifted by approximately 20 nm. For n-type SiNCs there is a significant reduction in PL intensity after 7 days, while for p-type SiNCs there was a slight increase in PL intensity. The reduction in PL intensity for n-type SiNCs after 7 days is due to Si–O–Si back bond inward oxidation, which is not sufficiently prevented in n-type SiNCs, leading to strained bonds and a reduction in the size of the SiNC core, and thus the observed blue shift in the PL. The high stability observed in p-type SiNCs is due to a well-passivated surface of Si–O–R terminations which prevent back bond inward oxidation and provide good steric stability.

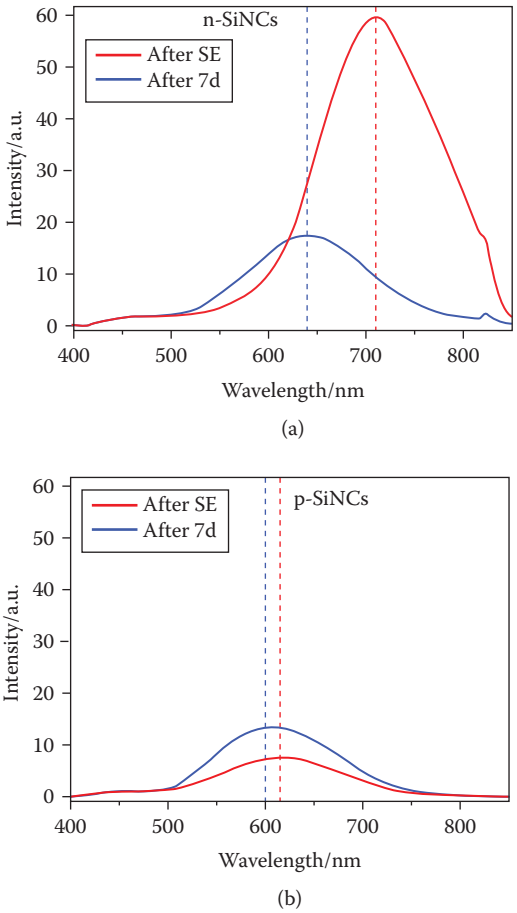

Figure 14.7 Photoluminescence (PL) spectra for SE silicon nanocrystals (SiNCs) following microplasma treatment in ethanol (red line) and after 7 days (blue line) for (a) n-type SiNCs SE for 60 minutes and (b) p-type SiNCs SE for 30 minutes, both in ethanol (the PL maxima is denoted by dotted lines in each spectra). (From Velusamy, T., et al., *ACS Appl. Mater. Interfaces* 7, 28207–28214, 2015.)

The effect of surface engineering on the Fermi level for n- and p-type SiNCs is demonstrated.[52] The position of the Fermi level was determined by scanning Kelvin probe, a technique which scans across a thin film and measures the contact potential difference between a conductive tip and sample surface, which can be translated into the Fermi level. The Fermi level is an important parameter for the design of photovoltaic devices, as this determines the energy band alignment and thus the barriers faced by carriers to travel between materials. The change in the Fermi level is attributed to changes in the surface terminations following surface engineering. Generally speaking, the formation of Si–O surface bonds leads to a change in the Fermi level due to a greater electronegativity of O compared to Si, leading to a shift in electrons from the Si to the O atoms and creating a surface dipole. These results confirm that the plasma–liquid surface engineering technique is not a "one size fits all" method. Different techniques must be developed for intrinsic, p-type, and n-type which are capable of achieving stable SiNCs with controllable and desirable properties.

14.4 SURFACE-ENGINEERED SiNC IN PHOTOVOLTAIC DEVICES

Organic PV have now surpassed 12% power conversion efficiency (PCE),[60] and present a potentially low-cost alternative to the conventional inorganic photovoltaic cells. The best cells are typically based on a bulk-heterojunction architecture, where the active layer consists of a mixture of conjugated donor and fullerene acceptor polymers. Organic solar cells are fabricated using polymers which can be deposited from solution via low-cost printing or coating techniques. These solution-phase coating methods can significantly reduce the cost of manufacture as they can be carried out without the need for high-temperature or high-vacuum atmospheres. There are two types of organic solar cells: (1) the organic bulk-heterojunction solar cell[61–63] based on an electron acceptor and a hole conductor, and (2) the dye-sensitized solar cell[64] based on a photo-anode sensitized by a dye, and an electrolyte for charge transfer.

The major challenge for organic photovoltaic devices such as the bulk-heterojunction cell surrounds the fullerene acceptor. Fullerenes are weak absorbers of visible light, their energy structure is difficult to tune, and production is both difficult and energy intensive. As well as this, fullerenes are unstable within the polymer matrix: fullerene molecules are prone to aggregate within the active layer of the solar cell device leading to a decrease in performance. The formation of large fullerene domains occurs via polymer diffusion which inhibits efficient electron collection. Domain formation can be overcome to some extent through using cosolvents during the deposition process. Despite this, alternatives to fullerenes remain desirable, fueling research both into alternative organic electron acceptors[65] and the emergence of the new field of hybrid solar cells.[66]

In a hybrid solar cell, the fullerene is replaced by an inorganic nanoparticle, typically a quantum-confined nanocrystal. This presents many opportunities to produce high-efficiency devices via band gap tuning, down conversion, and the much sought-after carrier multiplication, while still retaining the advantages of using low-cost and highly customizable organic donors. Plus, nanocrystals are typically much more absorbent than fullerenes, owing to increased contribution to device performance.

Semiconductor nanocrystals have a far broader absorption spectrum than organic compounds, can be doped p- or n-type, and have high surface-to-volume ratio providing a large interfacial area between QDs and the organic compound. Hybrid solar cells based on SiNCs with organic semiconductors have been reported,[2,67–70] most commonly in a bulk-heterojunction architecture. Liu et al. reported a hybrid solar cell based on SiNCs and poly(3-hexylthiophene) (P3HT) with a remarkable PCE of 1.15%[67] by direct replacement of the fullerene with SiNCs. In this case, the SiNCs were produced by nonthermal RF plasma from an SiH_4 precursor, and collection and handling was carried out in a nitrogen glovebox to reduce oxidation. This method expectedly yields H-terminated SiNCs due to the use of the SiH_4 precursor. Three groups of SiNCs were produced with diameters 3–5 nm, 5–9 nm, and 10–20 nm, with the smallest range of SiNCs producing the most efficient devices, likely due to reduced surface traps. Following this, Ding et al. reported a surface-engineered SiNC hybrid solar cell with PCE up to 2.2%.[68] Here, Cl-terminated SiNCs were etched to obtain H-terminated SiNCs. This work was followed up by the same group, who found that a loosely controlled oxidation process over a period of 12 hours yielded SiNC hybrid devices with 3.6% PCE. The oxidation process replaced dangling bonds with Si–O–Si bridge bonds, reducing the amount of

trap sites on the SiNC surface. However, excessive oxidation (>12 hr) led to a reduction in PCE, attributed to a deterioration in electrical properties. This work can be tentatively categorized as surface engineering of SiNCs, however, since the SiNCs were simply exposed to oxygen for a given amount of time, this type of method will most probably present issues in reproducibility.

Surface engineering via plasma-induced liquid chemistry has been shown to enhance the performance of SiNC solar cells in a SiNC/polymer hybrid cell. Švrček et al. reported an improvement in solar cell performance for devices produced with surface-engineered SiNCs when compared with as-prepared SiNCs.[69] SiNCs were synthesized by the electrochemical etching of a p-type Si wafer yielding H-terminated SiNCs. Surface engineering by DC microplasma was carried out on the colloidal solution as a means to passivate the SiNC surface. The Si–H terminations along with surface defects are mostly transformed into Si–O–R terminations. This surface engineering led to an enhancement in the PCE, and can be observed in the external quantum efficiency shown in Figure 14.8. This is due to an enhanced exciton dissociation at the polymer interface due to the SiNC surface. While the PCE of the device is low (0.03%), the surface engineering provided to be a 150% improvement in the PCE when compared with untreated SiNCs.

Velusamy et al. also reported SiNC test devices based on both p-type and n-type surface-engineered SiNCs. These test devices were fabricated to gain an understanding of the effect of the surface engineering on the device properties for p- and n-type SiNCs. There was an enhancement in efficiency for p-type surface-engineered SiNCs from 0.002 to 0.005% PCE, mostly attributed to an enhanced fill factor. However, for n-type SiNCs there was a substantial decrease in PCE from 0.01 to 0.001%, attributed to a fall in J_{SC}. The reduced J_{SC} is likely due to the oxide layer, which when too thick can reduce the electrical properties; here the electron mobility was reduced. It is therefore necessary to improve control over the surface engineering process such that the thickness of the oxide layer can be optimized and stabilized, leading to favorable electrical properties.

Figure 14.9 is a schematic diagram displaying the n- and p-type doped silicon nanocrystal Fermi level engineering for the improvement in band alignment in solar cells. The device architecture is taken from the literature for a typical hybrid silicon nanocrystal solar cell.[2] The control of the degree of oxidation via RF microplasma, and thus the control of the Fermi level and electronic transport properties, can be employed to enhance band alignment and increase solar cell device performance. It is also possible to achieve a surfactant-free type-I or type-II alignment (Figure 14.3) through surface engineering. Controlled modification of the surface oxidation can lead to a band alignment in which carriers are either confined to the core, or transported to surface states where they are either extracted or recombine.

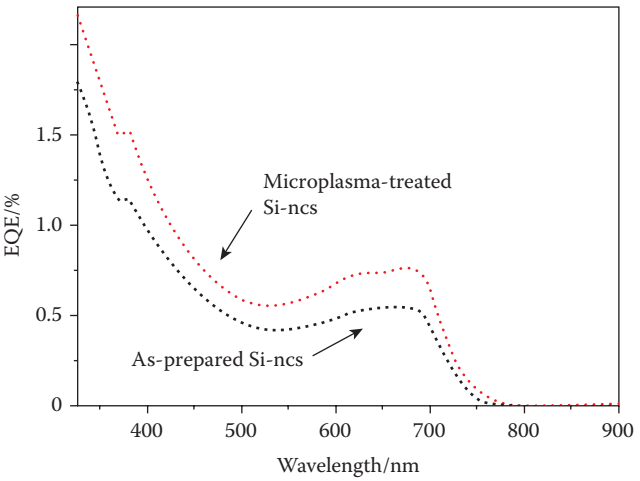

Figure 14.8 External quantum efficiency for a SiNC/PTB7 hybrid solar cell. Surface engineering by microplasma was observed to enhance the external quantum efficiency, and therefore provide an increase in the PCE. (From Švrček, V., et al., *Appl. Phys. Lett.*, 100, 223904, 2012.)

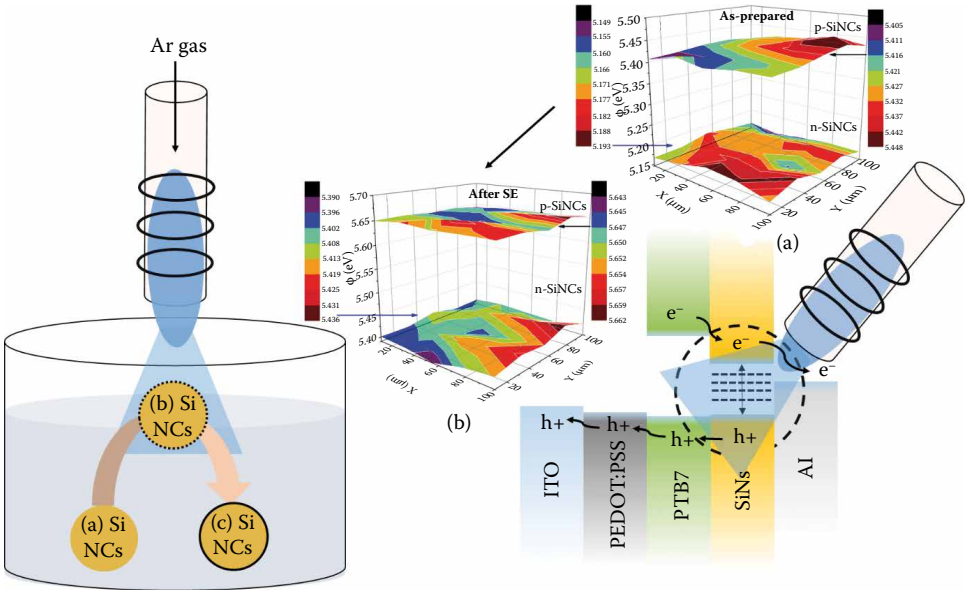

Figure 14.9 Schematic diagram displaying the silicon nanocrystals Fermi level engineering for improvement in band alignment in solar cells. The control of the degree of oxidation via RF microplasma, and thus the control of the Fermi level and electronic transport properties, can be employed to enhance band alignment and increase solar cell device performance. (Adapted from Velusamy, T., et al., *ACS Appl. Mater. Interfaces* 7, 28207–28214, 2015.)

14.5 CONCLUSION

In this chapter, we have overviewed doped SiNC surface engineering by plasma-induced chemistry that can significantly modify absorption and emission properties. The control of SiNC surface properties is highly important for producing useful nanocrystals for electronic and PV devices, while silicon itself possess many desirable features both physically and economically. We demonstrated that the plasma-induced surface chemistry at quantum confinement size is a powerful and flexible tool for the modification of surface chemistries of any nanocrystals, and can be achieved through DC, high-frequency, or laser processes in liquid media. These methods of surface engineering by plasma are particularly interesting given that they can be performed at atmospheric pressures, which is highly favorable for the incorporation into industry.

ACKNOWLEDGMENT

This work was partially supported by a NEDO projects, the Levehulme international network (IN-2012-136) and EPSRC (EP/K022237/1 and EP/M024938/1).

REFERENCES

1. Zhou, Z., Brus, L. & Friesner, R. Electronic structure and luminescence of 1.1- and 1. 4-nm silicon nanocrystals: Oxide shell versus hydrogen passivation. *Nano Lett.* **3**, 163–167 (2003).
2. Ding, Y., Sugaya, M., Liu, Q., Zhou, S. & Nozaki, T. Oxygen passivation of silicon nanocrystals: Influences on trap states, electron mobility, and hybrid solar cell performance. *Nano Energ.* **10**, 322–328 (2014).
3. Kim, K.-H. et al. Enhancement of light extraction from a silicon quantum dot light-emitting diode containing a rugged surface pattern. *Appl. Phys. Lett.* **89**, 191120 (2006).
4. Lien, Y.-C. et al. Fast programming metal-gate Si quantum dot nonvolatile memory using green nanosecond laser spike annealing. *Appl. Phys. Lett.* **100**, 143501 (2012).
5. Conibeer, G., Perez-Wurfl, I., Hao, X., Di, D. & Lin, D. Si solid-state quantum dot-based materials for tandem solar cells. *Nanoscale Res. Lett.* **7**, 193 (2012).
6. Conibeer, G. et al. Silicon quantum dot nanostructures for tandem photovoltaic cells. *Thin Solid Films* **516**, 6748–6756 (2008).

7. Lee, S., Lee, Y., Song, E. B. & Hiramoto, T. Observation of single electron transport via multiple quantum states of a silicon quantum dot at room temperature. *Nano Lett.* **14**, 71–77 (2013).
8. Chan, K. W. et al. Single-electron shuttle based on a silicon quantum dot. *Appl. Phys. Lett.* **98**, 212103 (2011).
9. Rokhinson, L. P., Guo, L. J., Chou, S. Y. & Tsui, D. C. Spintronics with Si quantum dots. *Microelectron. Eng.* **63**, 147–153 (2002).
10. de Boer, W. D. et al. Red spectral shift and enhanced quantum efficiency in phonon-free photoluminescence from silicon nanocrystals. *Nat. Nanotechnol.* **5**, 878–884 (2010).
11. Canham, L. T. Silicon quantum wire array fabrication by electrochemical and chemical dissolution of wafers. *Appl. Phys. Lett.* **57**, 1046–1048 (1990).
12. Iyer, S. S. & Xie, Y. H. Light emission from silicon. *Science* **260**, 40–46 (1993).
13. Hannah, D. C. et al. On the origin of photoluminescence in silicon nanocrystals: Pressure-dependent structural and optical studies. *Nano Lett.* **12**, 4200–4205 (2012).
14. Kanemitsu, Y. Luminescence properties of nanometer-sized Si crystallites: Core and surface states. *Phys. Rev. B* **49**, 16845–16848 (1994).
15. Puzder, A., Williamson, A. J., Grossman, J. C. & Galli, G. Surface chemistry of silicon nanoclusters. *Phys. Rev. Lett.* **88**, 097401 (2002).
16. Reboredo, F. A. & Galli, G. Theory of alkyl-terminated silicon quantum dots. *J. Phys. Chem. B* **109**, 1072–1078 (2005).
17. Godefroo, S. et al. Classification and control of the origin of photoluminescence from Si nanocrystals. *Nat. Nanotechnol.* **3**, 174–178 (2008).
18. Kovalev, D., Diener, J., Heckler, H., Polisski, G., Künzner, N. & Koch, F. Optical absorption cross sections of Si nanocrystals. *Phys. Rev. B* **61**, 4485–4487 (2000).
19. Kovalev, D., Heckler, H., Ben-Chorin, M., Polisski, G., Schwartzkopff, M. & Koch, F. Breakdown of the k-conservation rule in Si nanocrystals. *Phys. Rev. Lett.* **81**, 2803–2806 (1998).
20. Kůsová, K. et al. Brightly luminescent organically capped silicon nanocrystals fabricated at room temperature and atmospheric pressure. *ACS Nano* **4**, 4495–4504 (2010).
21. Groenewegen, V., Kuntermann, V., Haarer, D., Kunz, M. & Kryschi, C. Excited-state relaxation dynamics of 3-vinylthiophene-terminated silicon quantum dots. *J. Phys. Chem. C* **114**, 11693–11698 (2010).
22. Wilson, W. L., Szajowski, P. F. & Brus, L. E. Quantum confinement in size-selected, surface-oxidized silicon nanocrystals. *Science* **262**, 1242–1244 (1993).
23. English, D. S., Pell, L. E., Yu, Z., Barbara, P. F. & Korgel, B. A. Size tunable visible luminescence from individual organic monolayer stabilized silicon nanocrystal quantum dots. *Nano Lett.* **2**, 681–685 (2002).
24. Sykora, M., Mangolini, L., Schaller, R. D., Kortshagen, U., Jurbergs, D. & Klimov, V. I. Size-dependent intrinsic radiative decay rates of silicon nanocrystals at large confinement energies. *Phys. Rev. Lett.* **100**, 067401 (2008).
25. Mastronardi, M. L. et al. Preparation of monodisperse silicon nanocrystals using density gradient ultracentrifugation. *J. Am. Chem. Soc.* **133**, 11928–11931 (2011).
26. Belomoin, G. et al. Observation of a magic discrete family of ultrabright Si nanoparticles. *Appl. Phys. Lett.* **80**, 841 (2002).
27. Mastronardi, M. L. et al. Size-dependent absolute quantum yields for size-separated colloidally-stable silicon nanocrystals. *Nano Lett.* **12**, 337–342 (2012).
28. Shirahata, N. Colloidal Si nanocrystals: A controlled organic–inorganic interface and its implications of color-tuning and chemical design toward sophisticated architectures. *Phys. Chem. Chem. Phys.* **13**, 7284 (2011).
29. Wolkin, M. V., Jorne, J., Fauchet, P. M., Allan, G. & Delerue, C. Electronic states and luminescence in porous silicon quantum dots: The role of oxygen. *Phys. Rev. Lett.* **82**, 197–200 (1999).
30. Žídek, K. et al. Femtosecond luminescence spectroscopy of core states in silicon nanocrystals. *Opt. Express* **18**, 25241–25249 (2010).
31. Dasog, M., Bader, K. & Veinot, J. G. C. Influence of halides on the optical properties of silicon quantum dots. *Chem. Mater.* **27**, 1153–1156 (2015).
32. Yoffe, A. D. Low-dimensional systems: Quantum size effects and electronic properties of semiconductor microcrystallites (zero-dimensional systems) and some quasi-two-dimensional systems. *Adv. Phys.* **42**, 173–262 (1993).
33. Holmes, J. D., Ziegler, K. J., Doty, R. C., Pell, L. E., Johnston, K. P. & Korgel, B. A. Highly luminescent silicon nanocrystals with discrete optical transitions. *J. Am. Chem. Soc.* **123**, 3743–3748 (2001).
34. Jurbergs, D., Rogojina, E., Mangolini, L. & Kortshagen, U. Silicon nanocrystals with ensemble quantum yields exceeding 60%. *Appl. Phys. Lett.* **88**, 233116 (2006).
35. Bulutay, C. Interband, intraband and excited-state direct photon absorption of silicon and germanium nanocrystals embedded in a wide band-gap lattice. *Phys. Rev. B* **76**, 205321 (2007). doi: http://dx.doi.org/10.1103/PhysRevB.76.205321.

36. Öğüt, S., Chelikowsky, J. R. & Louie, S. G. Quantum confinement and optical gaps in Si nanocrystals. *Phys. Rev. Lett.* **79**, 1770–1773 (1997).
37. Vasiliev, I., Öğüt, S. & Chelikowsky, J. R. *Ab initio* absorption spectra and optical gaps in nanocrystalline silicon. *Phys. Rev. Lett.* **86**, 1813–1816 (2001).
38. Furukawa, S. & Miyasato, T. Quantum size effects on the optical band gap of microcrystalline Si:H. *Phys. Rev. B* **38**, 5726–5729 (1988).
39. Lockwood, D., Lu, Z. & Baribeau, J. Quantum confined luminescence in Si/SiO2 superlattices. *Phys. Rev. Lett.* **76**, 539–541 (1996).
40. Zhou, T. et al. Bandgap tuning of silicon quantum dots by surface functionalization with conjugated organic groups. *Nano Lett.* **15**, 3657–3663 (2015).
41. Gupta, A., Swihart, M. T. & Wiggers, H. Plasma nanoparticle synthesis: Luminescent colloidal dispersion of silicon quantum dots from microwave plasma synthesis: Exploring the photoluminescence behavior across the visible spectrum. *Adv. Funct. Mater.* **19**, 696–703 (2009).
42. Cheng, K.-Y., Anthony, R., Kortshagen, U. R. & Holmes, R. J. High-efficiency silicon nanocrystal light-emitting devices. *Nano Lett.* **11**, 1952–1956 (2011).
43. Baldwin, R. K., Pettigrew, K. A., Ratai, E., Augustine, M. P. & Kauzlarich, S. M. Solution reduction synthesis of surface stabilized silicon nanoparticles. *Chem. Commun.* **23**, 1822–1823 (2002).
44. Nolan, B. M., Henneberger, T., Waibel, M., Fässler, T. F. & Kauzlarich, S. M. Silicon nanoparticles by the oxidation of $[Si_4]^{4-}$—And $[Si_9]^{4-}$-containing Zintl phases and their corresponding yield. *Inorg. Chem.* **54**, 396–401 (2015).
45. Huang, S. Y. et al. Customizing electron confinement in plasma-assembled Si/AlN nanodots for solar cell applications. *Phys. Plasmas* **16**, 123504 (2009).
46. Kortshagen, U. Nonthermal plasma synthesis of semiconductor nanocrystals. *J. Phys. D. Appl. Phys.* **42**, 113001 (2009).
47. Mariotti, D. & Sankaran, R. M. Microplasmas for nanomaterials synthesis. *J. Phys. D. Appl. Phys.* **43**, 323001 (2010).
48. Nozaki, T., Sasaki, K., Ogino, T., Asahi, D. & Okazaki, K. Microplasma synthesis of tunable photoluminescent silicon nanocrystals. *Nanotechnology* **18**, 235603 (2007).
49. Sankaran, R. M., Holunga, D., Flagan, R. C. & Giapis, K. P. Synthesis of blue luminescent Si nanoparticles using atmospheric-pressure microdischarges. *Nano Lett.* **5**, 537–541 (2005).
50. Sato, S. & Swihart, M. T. Propionic-acid-terminated silicon nanoparticles: Synthesis and optical characterization. *Chem. Mater.* **18**, 4083–4088 (2006).
51. Švrček, V. Ex situ prepared Si nanocrystals embedded in silica glass: Formation and characterization. *J. Appl. Phys.* **95**, 3158 (2004).
52. Li, H., Wu, Z., Zhou, T., Sellinger, A. & Lusk, M. T. Tailoring the optical gap of silicon quantum dots without changing their size. *Phys. Chem. Chem. Phys.* **16**, 19275–19281 (2014).
53. Wang, G. et al. Type-II core-shell Si-CdS nanocrystals: Synthesis and spectroscopic and electrical properties. *Chem. Commun. (Camb).* **50**, 11922–11925 (2014).
54. Mariotti, D., Mitra, S. & Švrček, V. Surface-engineered silicon nanocrystals. *Nanoscale* **5**, 1385 (2013).
55. Mitra, S., Švrček, V., Mariotti, D., Velusamy, T., Matsubara, K. & Kondo, M. Microplasma-induced liquid chemistry for stabilizing of silicon nanocrystals optical properties in water. *Plasma Process. Polym.* **11**, 158–163 (2014).
56. Mariotti, D., Švrcek, V., Hamilton. W. J., Schmidt, M. & Kondo, M. Silicon nanocrystals in liquid media: Optical properties and surface stabilization by microplasma induced non equilibrium liquid chemistry. *Adv. Funct. Mater.* **22**, 954–961 (2012).
57. Svrcek, V. et al. Dramatic enhancement of photoluminescence quantum yields for surface-engineered Si nanocrystals within the solar spectrum. *Adv. Funct. Mater.* **23**, 6051–6058 (2013).
58. Švrcek, V., Mariotti, D. & Kondo, M. Microplasma-induced surface engineering of silicon nanocrystals in colloidal dispersion. *Appl. Phys. Lett.* **97**, 161502/1–161502/3 (2010).
59. Velusamy, T., Mitra, S., Macias-Montero, M., Svrcek, V. & Mariotti, D. Varying surface chemistries for p-doped and n-doped silicon nanocrystals and impact on photovoltaic devices. *ACS Appl. Mater. Interfaces* **7**, 28207–28214 (2015).
60. S. S. Li., Y. Li., W. C. Zhao., S. Q. Zhang., S. Mukherjee., H. Ade., and J. H. Hou. Energy-Level Modulation of Small-Molecule Electron Acceptors to Achieve over 12% Efficiency in Polymer Solar Cells. *Adv. Mater.* 28, 9423-9429 (2016)..
61. Yu, G., Gao, J., Hummelen, J. C., Wudl, F. & Heeger, A. J. Polymer photovoltaic cells: Enhanced efficiencies via a network of internal donor-acceptor heterojunctions. *Science* **270**, 1789–1791 (1995).
62. Halls, J. J. M. et al. Efficient photodiodes from interpenetrating polymer networks. *Nature* **376**, 498–500 (1995).

63. Park, S. H. et al. Bulk heterojunction solar cells with internal quantum efficiency approaching 100%. *Nat. Photonics* **3**, 297–302 (2009).
64. O'Regan, B. & Grätzel, M. A low-cost, high-efficiency solar cell based on dye-sensitized colloidal TiO_2 films. *Nature* **353**, 737–740 (1991).
65. Sauvé, G. & Fernando, R. Beyond fullerenes: Designing alternative molecular electron acceptors for solution-processable bulk heterojunction organic photovoltaics. *J. Phys. Chem. Lett.* **6**, 3770–3780 (2015).
66. Milliron, D. J., Gur, I. & Alivisatos, A. P. Hybrid organic–nanocrystal solar cells. *MRS Bull.* **30**, 41–44 (2005).
67. Liu, C.-Y., Holman, Z. C. & Kortshagen, U. R. Hybrid solar cells from P3HT and silicon nanocrystals. *Nano Lett.* **9**, 449–452 (2009).
68. Ding, Y., Gresbacka, R., Liub, Q., Zhoua, S., Pic, X. & Nozakia, T. Silicon nanocrystal conjugated polymer hybrid solar cells with improved performance. *Nano Energ.* **9**, 25–31 (2014).
69. Švrček, V., Yamanari, T., Mariotti, D., Matsubara, K. & Kondo, M. Enhancement of hybrid solar cell performance by polythieno [3,4-b]thiophenebenzodithiophene and microplasma-induced surface engineering of silicon nanocrystals. *Appl. Phys. Lett.* **100**, 223904 (2012).
70. Zhao, S., Pi, X., Mercier, C., Yuan, Z., Sun, B. & Yang, D. Silicon-nanocrystal-incorporated ternary hybrid solar cells. *Nano Energ.* **26**, 305–312 (2016).